Electronic Supplementary Material (ESI) for Chemical Communications.

Constructing Single Atom Sites on Bipyridine Covalent Organic Frameworks for Selective Electrochemical Production of H_2O_2

Shaoda Huang[a,b], Bingyan Zhang[a], Huimin Sun[a], Hongyin Hu[a], Jinyan Wang[a], Fang Duan[a], Han Zhu[a], Mingliang Du[a], Shuanglong Lu[a*]

[a]*Key Laboratory of Synthetic and Biological Colloids, Ministry of Education, School of Chemical and Material Engineering, Jiangnan University, Wuxi, Jiangsu 214122, P. R. China. E-mail: lushuanglong@jiangnan.edu.cn*

[b]*School of Materials Science and Engineering, Natural Sciences and Science Education in National Institute of Education, Nanyang Technological University, Singapore, 637616 Singapore*.

Experimental

Material

The 4, 4′ , 4″ , 4‴-(pyrene-1,3,6,8-tetrayl)-tetraaniline (Py) and 2, 2′ -bipyridyl-5,5′ -dialdehyde (Bpy) were purchased from Jilin Chinese Academy of Sciences-Yanshen Technology Co., 1,4,-dioxane, mesitylene, acetic acid (AcOH), tetrahydrofuran, ethanol, methanol, and isopropanol were obtained from Shanghai Civi Chemical Technology Co.. Potassium hydroxide (KOH), Nafion solution, $M(CH_3COOH)_2$ ($(M(OAc)_2$) M= Mn, Fe, Co, Ni, Cu, and Zn) and carbon support were obtained from Aladdin Industrial Co. All the solvents were purchased and used as received without further purification.

Characterizations

The morphology and structure of samples were characterized using field-emission Field emission scanning electron microscopies (SEM) and corresponding elemental analysis measurements (S-4800), TEM (JEM-2100plus). Aberration-corrected HAADF-STEM was performed using a FEI Themis Z microscope (Titan Cubed Themis G2300). Powder X-ray diffraction (PXRD) analysis was performed on Bruker DAVINCI diffractometer using Cu Kα radiation. X-ray photoelectron spectroscopy (XPS) measurements were carried out on a Thermo Scientific K-Alpha spectrometer. FT-IR spectra were obtained from a Nicolet 6700 spectrometer. Inductively Coupled Plasma-Atomic Emission Spectrometry (ICP-AES) (PerkinElmer 8300) analyses were used to determine the mass concentration of metal in samples. The Brunauer–Emmett–Teller (BET) specific surface area was measured by nitrogen adsorption at 77 K on a surface area (ASAP2020 MP). Thermogravimetric analysis (TGA) was carried out on TGA1100SF setup from 100 to 800 ℃ under N_2 atmosphere with a ramp rate of 10 ℃ min^{-1}. Solid-state ^{13}C cross-polarization with magic-angle spinning (CP-MAS) NMR spectrum was collected on a Brucker 400 M spectrometer.

Synthesis of Py-Bpy-COF and Py-Bpy-COF-M

Synthesis of Py-Bpy-COF: A Pyrex tube (10 mL) was charged with Py (85.07 mg, 0.15 mmol) and Bpy (64.01 mg, 0.30 mmol), mesitylene (1.5 mL), 1,4-Dioxane (1.5 mL) and AcOH solution (500 µL, 3 M). The mixture was ultrasonicated for five minutes and then flash-frozen in a liquid N_2 bath and degassed through three freeze-pump-thaw cycles.[1] The tube was flame-sealed under a vacuum using a Schlenk line and oil pump. The tube was heated at 120 °C in an oven for 72 h. After cooling to room temperature, the orange product was successively washed with THF, water, and methanol, respectively. The resulting powder was subjected to Soxhlet extraction with THF for one day. The powder was collected and dried at 60 °C under a vacuum overnight to afford the target COF.

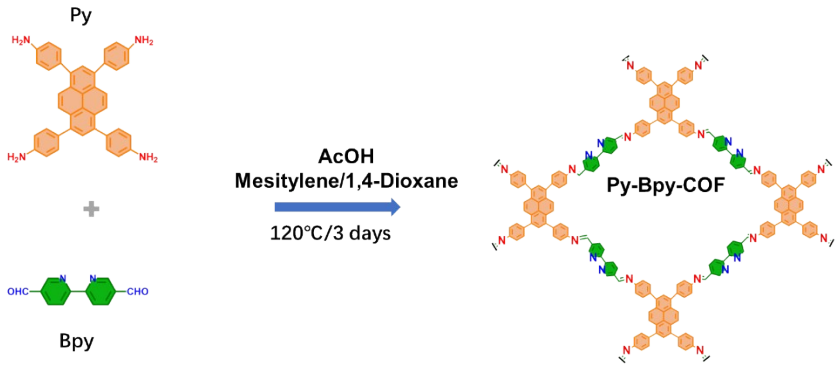

Synthesis of Py-Bpy-COF-M: Py-Bpy-COF (20 mg) was mixed with $M(OAc)_2$ (10 mg) in methanol (20 mL), and the resulting suspension was refluxed for 12 h. After this, the solid was filtered off

and washed with methanol. The resulting solid was dried under a vacuum at 60 °C overnight to yield Py-Bpy-COF-M (M= Mn, Fe, Co, Ni, Cu, and Zn).

Electrochemical measurements

An Iviumatat electrochemical workstation equipped with RRDE system was conducted for electrochemical measurement. A saturated calomel electrode (SCE) and a graphite rod were used as reference electrode and counter electrode. The inks of as-prepared catalysts were prepared by following procedure. Typically, 1.8 mg catalysts and 0.6 mg carbon support were added into a solution containing 200 ul isopropanol, 60 ul ultrapure water, and 10 ul Nafion solution, and then the mixed solution was sonicated for 30 minutes. 10 ul of catalyst's ink was dropped onto the glassy carbon electrode with a Pt ring acting as work electrode. The linear sweep voltammetry (LSV) plots were collected in O_2-saturated 0.1 M KOH solution with a scan rate 10 mv s^{-1} at the 1600 rpm. Long-term stability test was conducted at an applied potential of 0.55 V. All recorded potentials were converted into reversible hydrogen electrode (vs.RHE) based on the equation: E (RHE) = E (SCE)+0.244+0.0591pH equation.

The H_2O_2 selectivity and electron-transfer number (n) were calculated from the following function respectively:

$$H_2O_2(\%) = \frac{200I_R}{(I_D N + I_R)}$$

$$n = \frac{4I_D}{I_D + I_R N}$$

where I_D and I_R are the disk current and ring current, and N stands for the current collection efficiency of the Pt ring, which is determined to be 0.37.

The turnover frequency (TOF) and kinetic current density of the catalysts were calculated according to the following equations:

$$\frac{1}{J} = \frac{1}{J_L} + \frac{1}{J_K} = \frac{1}{B\omega^{\frac{1}{2}}} + \frac{1}{J_K}$$

$$B = 0.2nFC_0 D^{\frac{2}{3}} \gamma^{-\frac{1}{6}}$$

$$TOF = \frac{J_K * F(H_2O_2) * S_A}{n * N * F}$$

$$FE(H_2O_2/\%) = \frac{100I_R}{NI_D}$$

where J is the measured current density, J_L and J_K are the limiting and kinetic current densities, ω is the rotation speed of the electrode (rpm), n is the electron transfer number, F is the Faraday constant (96485 C mol^{-1}), C_0 is the bulk concentration of O_2 in 0.1 M KOH solution (1.2×10^{-6} mol cm^{-3}), D is the diffusion coefficient of O_2 ($1.9 \times$ 10-5 cm^2 s^{-1}) in 0.1 M KOH solution, and γ is the kinematic viscosity of the electrolyte (0.01 cm^2 s^{-1}).

FE (H_2O_2) is the faradaic efficiency of H_2O_2, S_A is the geometric surface area of the disk electrode. n is the electron-transfer number for the H_2O_2 production, N is the molar quantities of the electroactive component (metal loading amount) loaded on the disk electrode, and F is the Faraday constant (Ref. 16).

H_2O_2 quantification

The H_2O_2 concentration was measured by traditional cerium sulfate $Ce(SO_4)_2$ titration method

based on the mechanism that a yellow solution of Ce^{4+}would be reduced by H_2O_2 to colorless Ce^{3+} (1).

$2Ce^{4+} + H_2O_2 \rightarrow 2Ce^{3+} + 2H^+ + O_2$ (1)

Therefore, the concentration of H_2O_2 (M) can be determined by the following equation:

$M(H_2O_2) = 1/2\ \Delta M(Ce^{4+})$ (2)

Typically, the yellow transparent $Ce(SO_4)_2$ solution (1 mM) was prepared by dissolving 33.2 mg $Ce(SO_4)_2$ in 100 ml 0.5 M sulfuric acid solution. Then the collected electrolyte (400 ul) were titrated into 3 ml $Ce(SO_4)_2$ solution (1 mM) and shaking the mixed solution for two minutes. As a counterpart, the 400 ul 0.1 M KOH solution was titrated into 3 ml $Ce(SO_4)_2$ solution (1 mM) to obtain the mixed solution unreacted. Based on the linear relationship between the signal intensity of ultraviolet-visible spectroscopy (at around 316 nm) and Ce^{4+} concentration. The concentration of Ce^{4+} before and after the reaction can be measured by ultraviolet-visible spectroscopy. Therefore, the H_2O_2 concentrations of the samples could be obtained.

Zn-air battery assembly and test: A homemade Zn-air battery was constructed. The air cathode was prepared by coating the catalyst on carbon paper with a loading of 2 mg cm^{-2}. A polished Zn plate (thickness：1 mm) was employed as an anode and the void between the two electrodes was filled with 6 M KOH. An alkaline membrane was sandwiched between the electrodes to avoid the H_2O_2 to diffuse into the anode. The polarization curves and discharge were performed at 25 ℃ with the electrochemical working station.

Computational details.

All the density functional theory (DFT) calculations[2,3] were carried out in the DMol3 package of Materials Studio 2018. The exchange-correlation potential was treated by using a generalized gradient approximation (GGA) with the Perdew-Burke-Ernzerhof (PBE) parametrization.[4,5] A cutoff energy of 450 eV was set. The electronic energy was considered self-consistent when the energy change was smaller than 10^{-5} eV, while the tolerance convergence in ionic was 10^{-5} eV, too. Furthermore, the van der Waals correction of Grimme's DFT-D3 model was adopted.

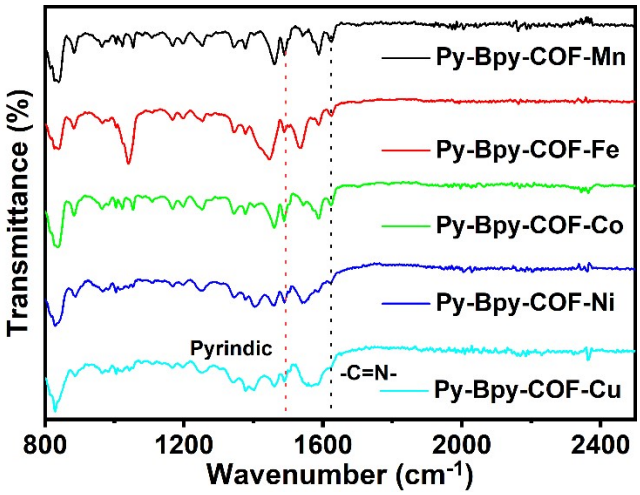

Fig. S1. FT-IR spectra of Py-BPy-COF-Mn, Fe, Co, Ni, Cu.

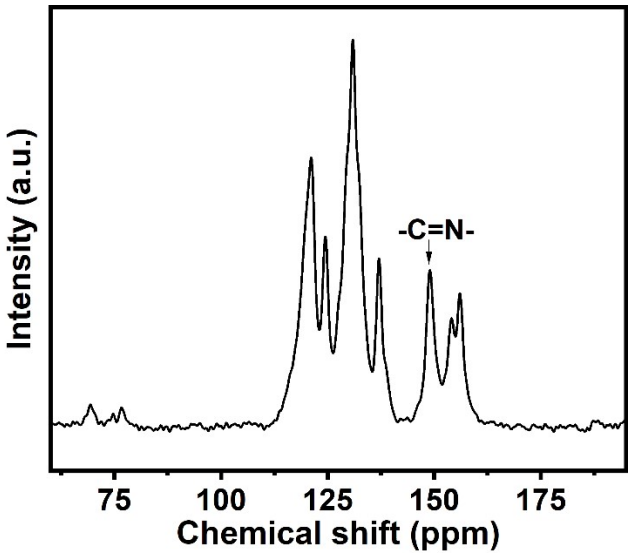

Fig. S2. Solid-state 13C NMR spectra of Py-Bpy-COF.

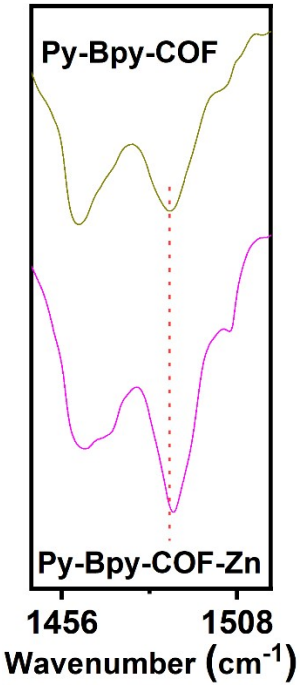

Fig. S3. The marked FT-IR spectra Fig 1.

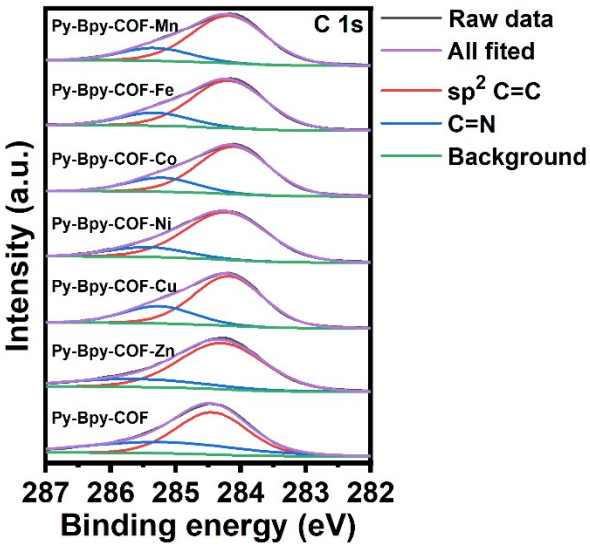

Fig. S4. C1s XPS spectra and their deconvolution of Py-Bpy- COF-M (M=Mn, Fe, Co, Ni, Cu, Zn).

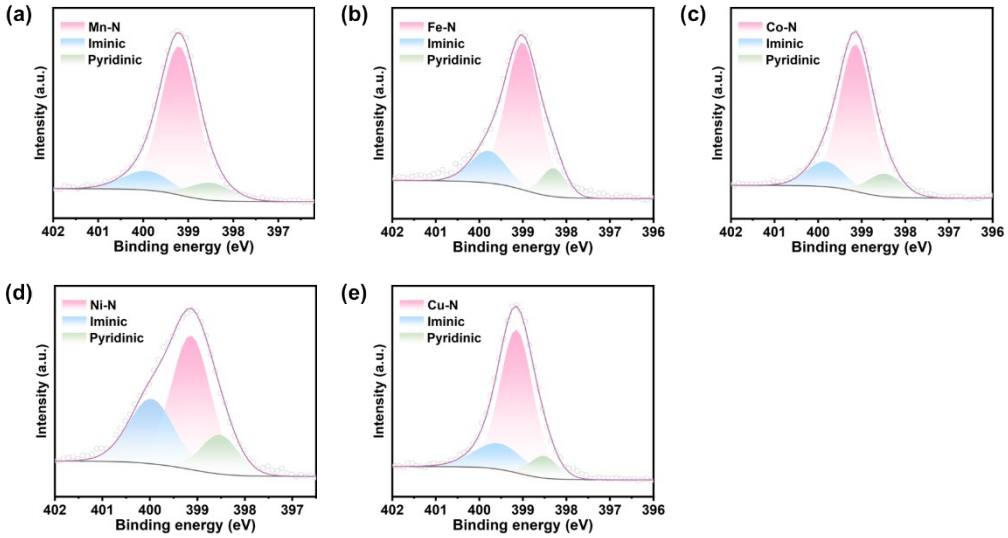

Fig. S5. N 1s XPS spectra and their deconvolution of Py-Bpy- COF-M (M=Mn, Fe, Co, Ni, Cu).

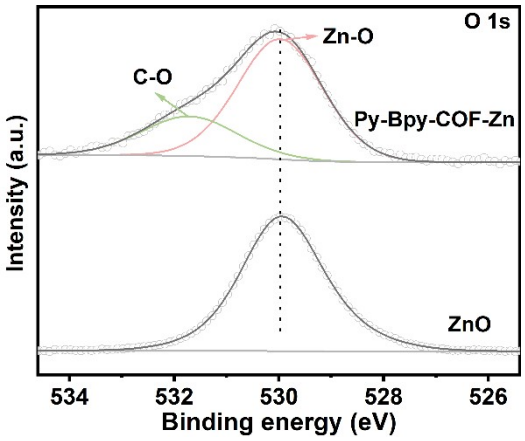

Fig. S6. O 1s XPS spectra of Py-Bpy-COF-Zn and ZnO.

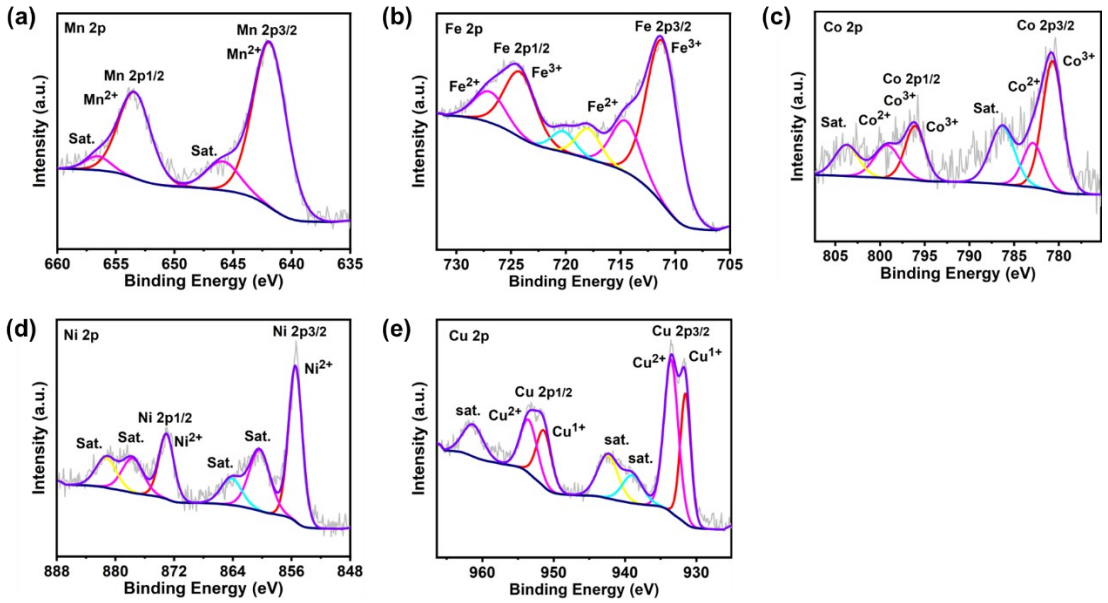

Fig. S7. Metal 2p XPS spectra and their deconvolution of Py-Bpy- COF-M (M=Mn, Fe, Co, Ni, Cu).

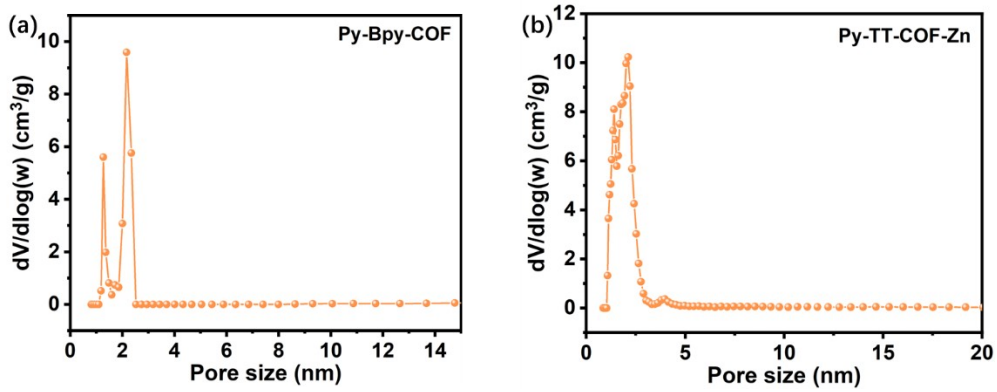

Fig. S8. The pore size distribution of Py-Bpy- COF and Py-Bpy- COF-Zn.

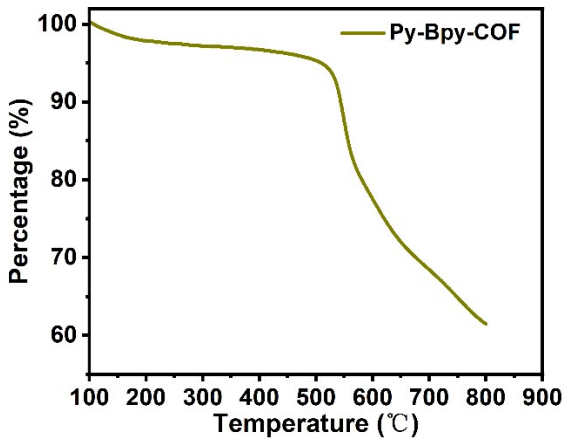

Fig. S9. The TGA analysis of Py-Bpy- COF.

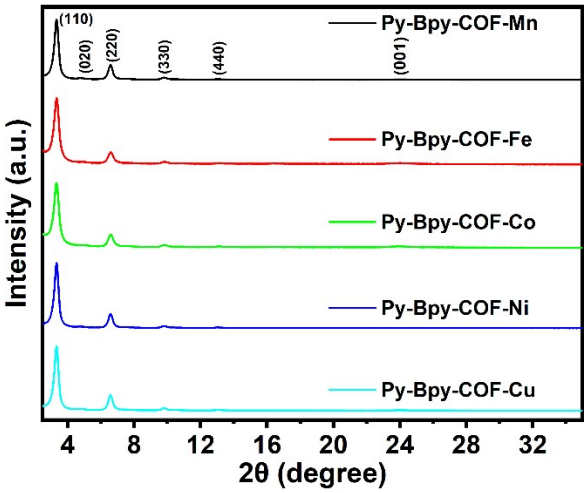

Fig. S10. XRD patterns of Py-Bpy- COF-M (M=Mn, Fe, Co, Ni, Cu).

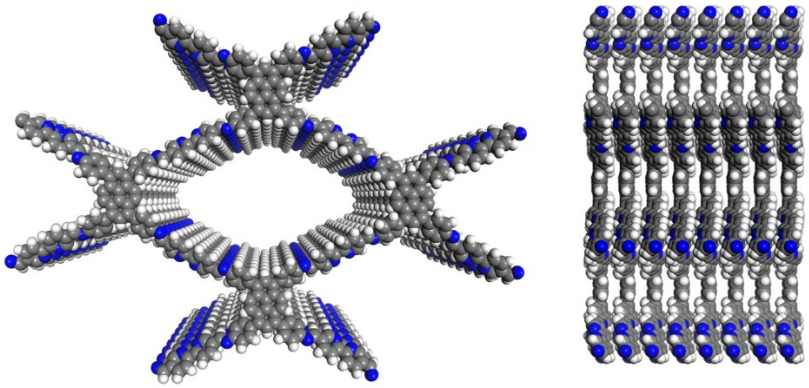

Fig. S11. Structural model of Py-Bpy- COF.

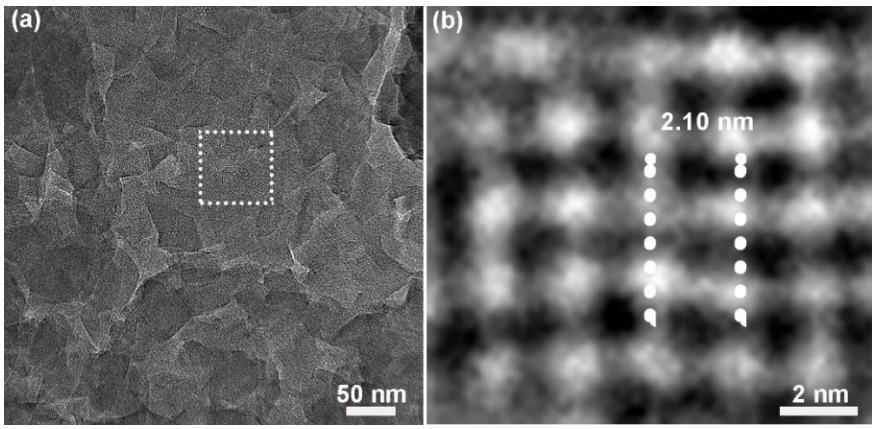

Fig. S12. HRTEM images of Py-Bpy- COF.

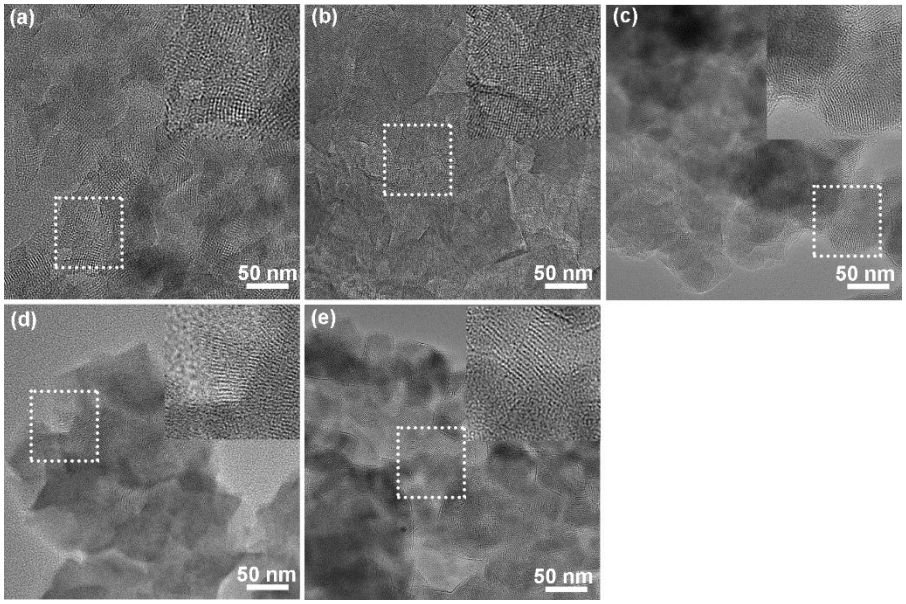

Fig. S13. HRTEM images of Py-Bpy- COF-M (M=Mn (a), Fe (b), Co (c), Ni (d), Cu(e)).

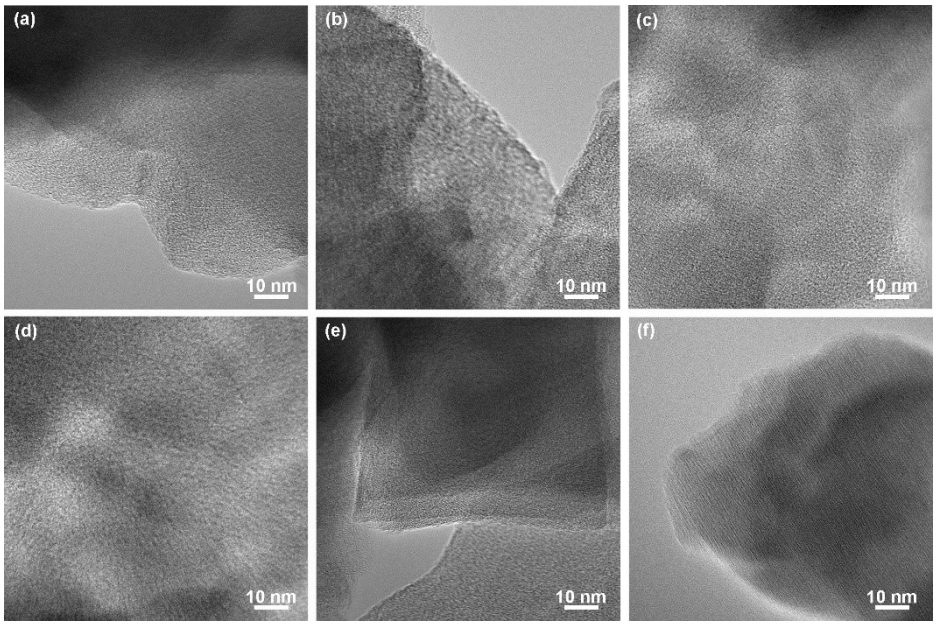

Fig. S14. HRTEM images of Py-Bpy- COF-M (M=Mn (a), Fe (b), Co (c), Ni (d), Cu(e), Zn (f)) with higher magnification.

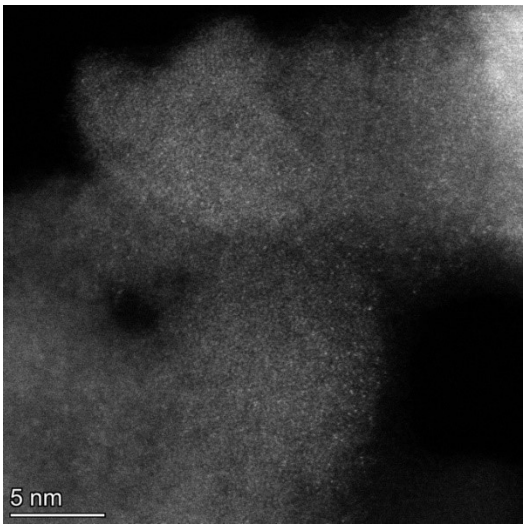

Fig. S15. Aberration-corrected HAADF-STEM image of Py-Bpy- COF-Zn.

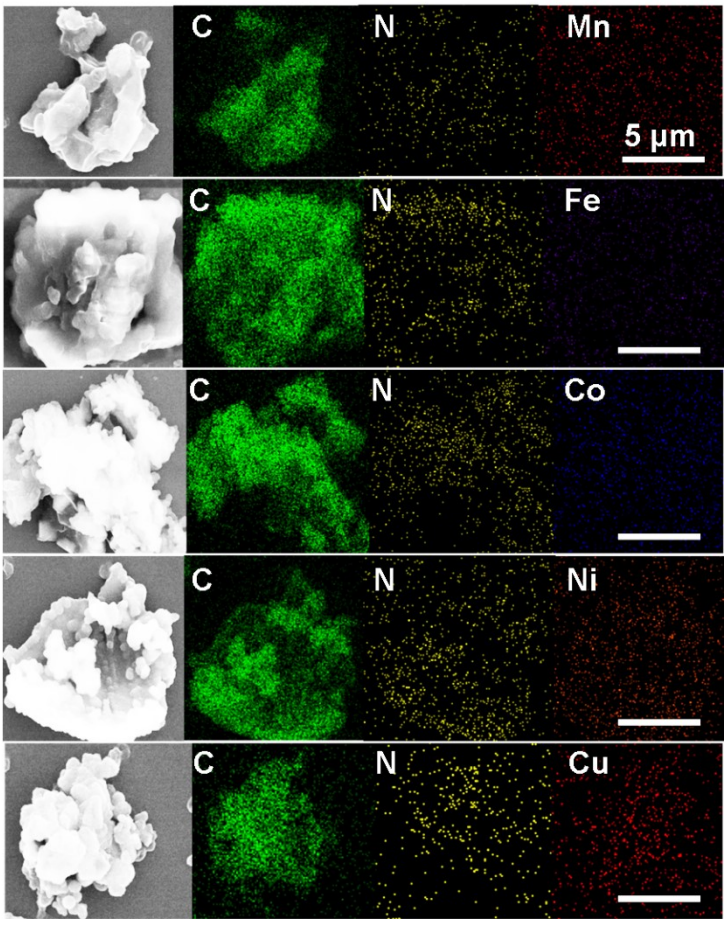

Fig. S16. Elemental analysis of Py-Bpy- COF-M (M=Mn, Fe, Co, Ni, Cu).

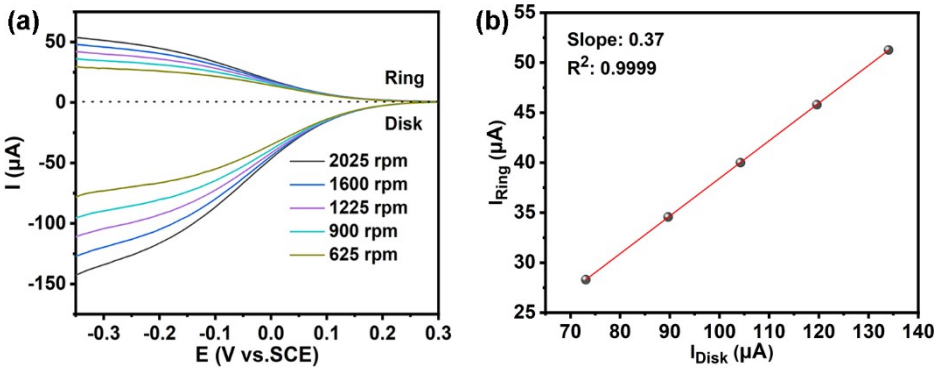

Fig. S17. (a) the Linear sweep voltammetry (LSV) curves were recorded on a bare glassy carbon rotation disk electrode with a Pt ring in 0.1 M KOH + 1 mM $K_3Fe(CN)_6$ with a sweep rate of 10 mV s^{-1} at the applied potential of 1.55 V (vs. RHE), (b) linear fitting of the diffusion-limited current densities recorded on ring and disk electrodes at the different rotation speed.

The apparent collection efficiency (N) was determined to be 0.37 in the ferrocyanide/ferricyanide half-reaction system at a rotation rate between 625 and 2025 rpm. Specifically, the Linear sweep voltammetry (LSV) curves were recorded on a bare glassy carbon rotation disk electrode with a Pt ring in 0.1 M KOH+1 mM $K_3Fe(CN)_6$ with a sweep rate of 10 mV s^{-1} at the applied potential of 1.55 V (vs. RHE) on the ring electrode, then the N can be determined based on linear fitting of the diffusion-limited current densities recorded on ring and disk electrodes at the different rotation speed.

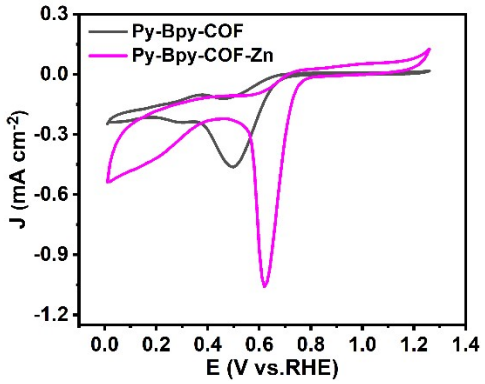

Fig. S18. The CV plots of the Py-Bpy-COF and Py-Bpy-COF-Zn in O_2-saturated 0.1 M KOH.

The cyclic voltammetry (CV) plots for the Py-Bpy-COF and Py-Bpy-COF-Zn were collected in the O_2-saturated 0.1 M KOH with 50 mv s^{-1} in the potential range of 0.01-1.26 V vs. RHE. As shown in Fig. S18, the Py-Bpy-COF-Zn shows a more positive and intensive reduction peak at approximately 0.62 V vs. RHE than that of Py-Bpy-COF, which indicates the higher ORR activity of Py-Bpy-COF-Zn.

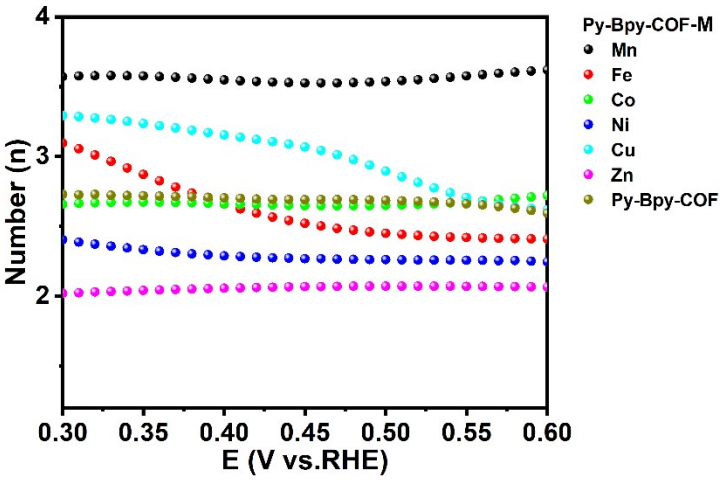

Fig. S19. The electron transfer number of Py-Bpy- COF and Py-Bpy- COF-M (M=Mn, Fe, Co, Ni, Cu, Zn).

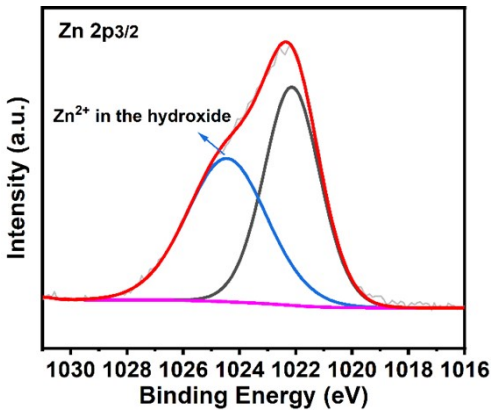

Fig. S20. Zn $2p_{3/2}$ XPS spectra of Py-Bpy-COF-Zn after the durability test.

During the durability test, a slight change in selectivity was observed when examining both the ring and disc electrodes. The gradual decay, particularly on the ring electrode, may be attributed to the poisoning of active sites by anions during the $2e^-$ ORR process (*Angew. Chem., Int. Ed* **2022**, *134*, e202117347).

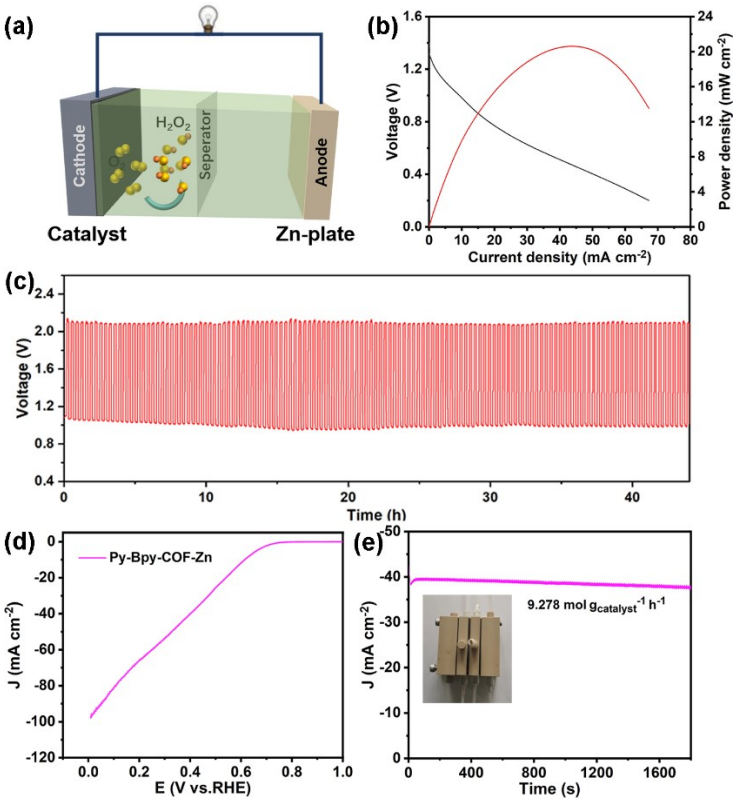

Fig. S21. (a) The model of Zn-air setup, (b) galvanostatic discharge voltage and power density curves, (c) charge−discharge cycling performance of Zn-air setup with Py-Bpy-COF-Zn catalyst, (d) LSV plot, (e) chronoamperometric test at the 0.3 V using flow cell.

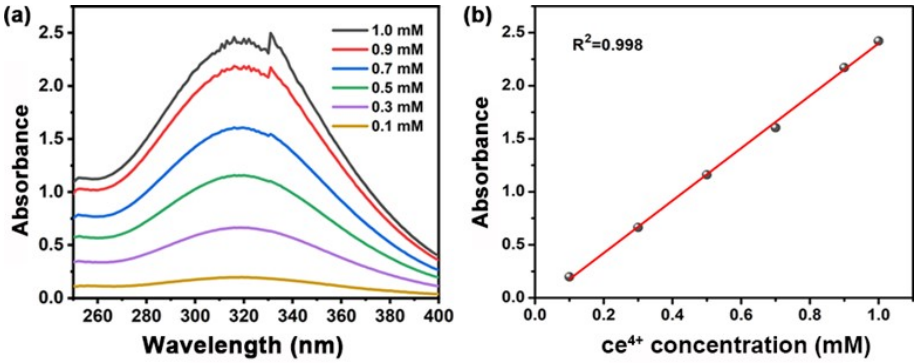

Fig. S22. A linear calibration curve was established by the Ce^{4+} absorbance at 316 nm from 0.1 to 1 mM.

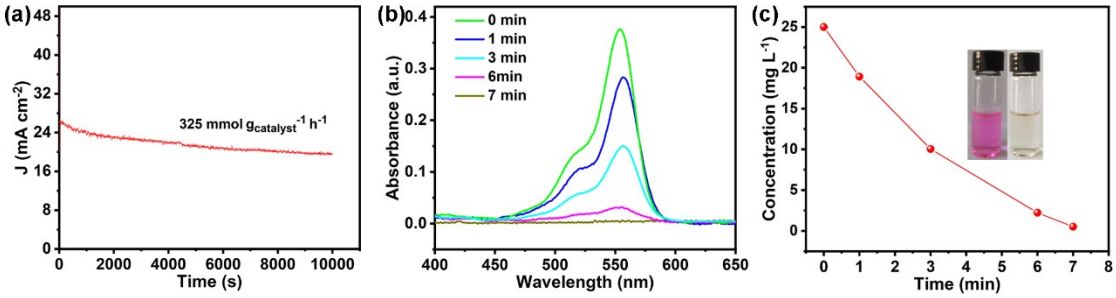

Fig. S23. (a) Discharge profile of the Zn−air battery at a constant potential of 0.8 V for 10000 s, (b) UV−Vis absorption spectra of acidic RhB solution treated by the collected electrolyte, (c) corresponding concentration changes of RhB over the treatment time.

The battery operated under a constant voltage of 0.8 V for a duration of 10000 s, yielding a stable current density of 20 mA cm^{-2}. The H_2O_2 production rate was calculated to be 325 mmol $g_{catlyst}^{-1}$ h^{-1} using a $Ce(SO_4)_2$ titration method (Fig. S21). Notably, the H_2O_2 concentration of the collected electrolyte is high enough to be directly utilized in the degradation of dye pollution in wastewater through the Fenton reaction. As a demonstration, a 5 mL catholyte after the electrolysis was added to a solution containing acidified Rhodamine B (Rh B, 25 mg L^{-1}) with 0.1 mmol Fe^{2+}. Upon easy hand-shaking, the color of the solution rapidly faded in several minutes, indicating the successful degradation of Rh B. It was further confirmed by the UV-vis absorption spectra that almost 100% of RhB was eliminated from the simulated wastewater after 7 minutes.

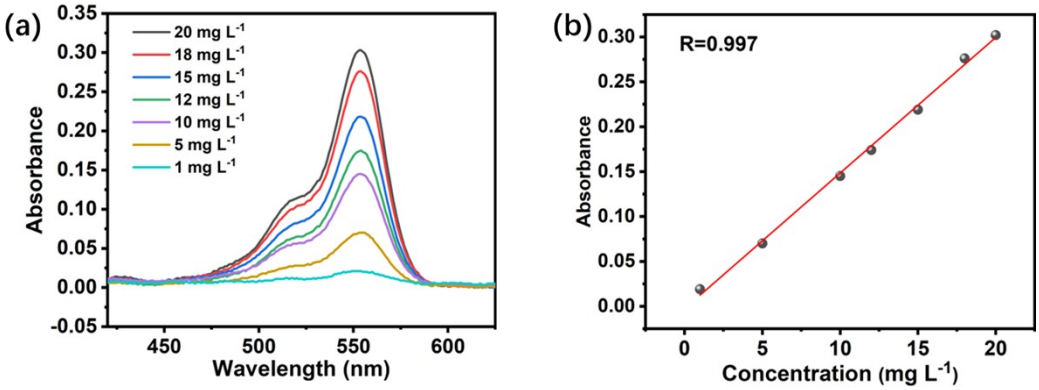

Fig. S24. (a) UV-vis absorption spectra of the calibration curves for RhB solution. (b) The fitting curves of the calibration signal for RhB.

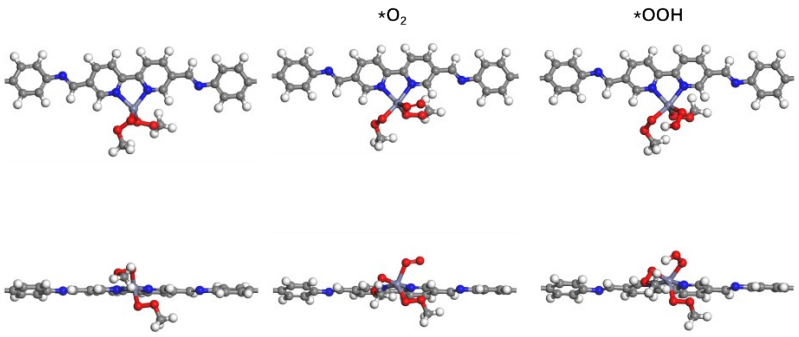

Fig. S25. Geometries of the adsorbed reaction intermediates on Py-Bpy- COF-Zn toward 2e- ORR.

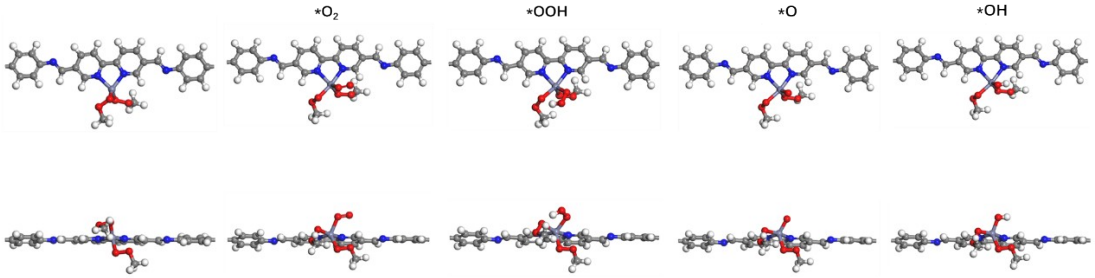

Fig. S26. Geometries of the adsorbed reaction intermediate on Py-Bpy- COF-Zn toward 4e- ORR.

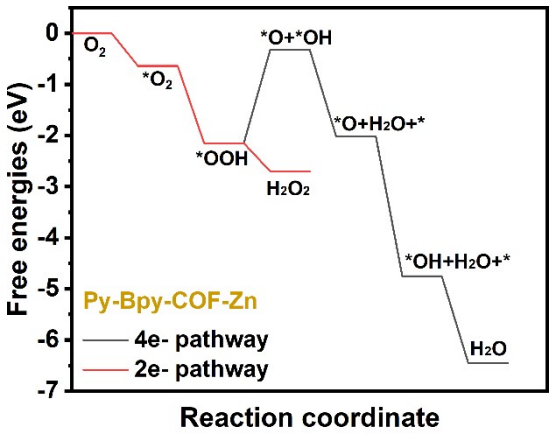

Fig. S27. Gibbs free energy of different intermediates on Py-Bpy- COF-Zn toward 2e- ORR and 4e- ORR.

Table S1. Metal loading in COF-366 and COF-366-M

Samples	Metal loading (at %)[a]	Metal loading (at %)[b]
Py-Bpy-COF-Mn	0.88	0.91
Py-Bpy-COF-Fe	1.12	1.16
Py-Bpy-COF-Co	1.21	1.25
Py-Bpy-COF-Ni	1.00	1.13
Py-Bpy-COF-Cu	0.93	0.98
Py-Bpy-COF-Zn	0.95	1.07

a: determined by XPS; b: determined by ICP-AES.

Table S2. The comparison of reported SACs toward electrocatalytic 2e$^-$ ORR for H_2O_2 production (NA: no analysis).

Catalysts	Electrolyte	Onset potential (V vs.RHE)	Selectivity (%)	H_2O_2 yield	Reference
By-Bpy-COF-Zn	**0.1 M KOH**	**0.78 V (vs.RHE)**	**99.1 (0.3 vs.RHE)**	**9.278 mol $g_{catalyst}^{-1}$ h^{-1} within 1800 s (40 mA cm^{-2}; Flow cell)**	**This work**
Mo_1/OSG-H	0.1 M KOH	~0.80 V (vs.RHE)	~95 % (0.55 vs.RHE)	NA	*Angew. Chem., Int. Ed.* 2020, 59, 9171.
Ni-N_2O_2/C	0.1 M KOH	~0.74 V (vs.RHE)	~96 % (0.45 V vs.RHE)	5.9 mol $g_{catalyst}^{-1}$ h^{-1} (70 mA cm^{-2}; flow cell)	*Angew. Chem., Int. Ed.* **2020**, 59, 13057.
O-C(Al)	0.1 M NaOH	~0.85 V (vs.RHE)	~96 % (0.55 V vs.RHE)	867 ppm within 3600 s (30 mA cm^{-2}; H-Cell)	*Nat. Commun.* **2020**, 11, 5478.
Fe-CNT	0.1 M KOH	~0.82 V (vs.RHE)	~95 (0.70 V vs.RHE)	1.6 mol $g_{catalyst}^{-1}$ h^{-1}(43 mA cm^{-2}; flow cell)	*Nat. Commun.* **2019**, 10, 3997.
Co–N–C	0.1 M KOH	~0.78 V (vs.RHE)	~82 % (0.1 V vs.RHE)	418 ±19 (50 mA; H-Cell)	*Nat. Mater.* **2020**, *19*, 436.
FeN_2O_2	0.1 M KOH	~0.79 V (vs.RHE)	~95 % (0.6 V vs.RHE)	300 mmol L^{-1} within 50 hours (60 mA cm^{-2}; gas-diffusion electrode)	*Appl. Catal., B* **2022**, 315, 121578.
CoN4-PC	0.1 M KOH	~0.81 V (vs.RHE)	~97 % (0.5 V vs.RHE)	11.2 mol $g_{catalyst}^{-1}$ h^{-1} within 110 hours (43 mA cm^{-2}; flow cell)	*Appl. Catal., B* **2023**, 324, 122267.
Co-SAs/NC	0.1 M KOH	~0.84 V (vs.RHE)	~76 % (0.5 V vs.RHE)	38.1 ± 1.5 mmol $g_{catalyst}^{-1}$ h^{-1} within 10 hours (3 mA)	*Inorg. Chem. Front.* **2021**, *8*, 2829.
Ni-SA/G	0.1 M KOH	~0.74 V	~94 (0.6 V	NA	*ACS Appl. Mater.*

		(vs.RHE)	vs.RHE)		*Interfaces* **2020**, 12, 15, 17519–17527.
In SAs/NSBC	0.1 M KOH	~0.78 V (vs.RHE)	~95 % (0.66 V vs.RHE)	6.49 mol $g_{catalyst}^{-1}$ h^{-1} within 12 hours (90 mA cm^{-2}; polymer electrolyte membrane fuel cell)	*Angew. Chem., Int. Ed.* 2022, 134, e202117347.
Zn-N_3O	0.1 M KOH	~0.72 V (vs.RHE)	~88 % (0.5 V vs.RHE)	248 mmol $g_{catalyst}^{-1}$ h^{-1} within 5 hours (2.5 mA cm^{-2}; H-cell)	*Chem. Eng. J.* **2023**, 455, 140721.
Co-N-C	0.1 M KOH	~0.83 V (vs.RHE)	~72 % (0.3 V vs.RHE)	4 mol $g_{catalyst}^{-1}$ h^{-1} within 6 hours (50 mA cm^{-2}; commercial microflow cell)	*J. Am. Chem. Soc.* **2019**, 141, 12372-12381.
W_1/NO-C	0.1 M KOH	~0.82 V (vs.RHE)	~90 % (0.6 V vs.RHE)	1.23 mol $g_{catalyst}^{-1}$ h^{-1} within 1 hours (13 mA cm^{-2}; H-cell)	*Adv. Funct. Mater.* 2022, 32, 2110224
COF-366-Co	0.1 M KOH	~0.72 V (vs.RHE)	~91 % (0.3 V vs.RHE)	909 mmol $g_{catalyst}^{-1}$ h^{-1} within 3 hours (22 mA cm^{-2}; H-cell)	*J. Am. Chem. Soc.* **2020**, 142, 21861-21871.

Reference

1. W. Leng, Y. Peng, J. Zhang, H. Lu, X. Feng, R. Ge, B. Dong, B. Wang, X. Hu and Y. Gao, *Chem. Eur. J.*, 2016, **22**, 9087-9091.
2. P. Hohenberg and W. J. P. r. Kohn, *Phys. Rev*. 1964, 136, B864.
3. W. Kohn and L. J. J. P. r. Sham, Phys. Rev. 1965, 140, A1133.
4. M. Ernzerhof and G. E. J. T. J. o. c. p. Scuseria, J. Chem. Phys. 1999, 110, 5029-5036.
5. B. Hammer, L. B. Hansen and J. K. J. P. r. B. Nørskov, Phys. Rev. B: Condens. Matter 1999, 59, 7413.